Chapter 3
Volterra Integral Equation Approach to the Electron Dynamics in Intense Optical Pulses

Yosuke Kayanuma

Abstract Recent advances in laser technology have made it possible to utilized very high intensity optical pulses with wide range of wave-length to pump electrons in materials. This opened a new era in experimental physics to use pulse-lasers as a tool to manipulate electrons not only for the ultrafast probe into electronic states in materials, but also for a new means to obtain light with much higher frequebecause it is morencies than the pump-pulse. From theoretical side, this requires to establish a coherent theoretical framework to analyze the ultra fast dynamics of the electrons driven by high intensity light fields. In this article, I propose a novel theoretical technique to approach this subject. We formulate the Volterra integral equations of second kind for that purpose. Although this is equivalent to the differential equations of Schrödinger, it has an advantage to treat the light-matter interactions as two independent modules; the intra-band driving and the inter-band driving. The expression for the former can be obtained analytically in many cases and is incorporated into the theory as an integral kernel. The formalism is applied to two simple models, the population inversion in the molecules under intense laser beams in air, and the high harmonic generations in solids.

3.1 Introduction

Thanks to the advances of high intensity and ultrashort laser technology, various new aspects of the quantum dynamics in the electronic excited states have been revealed. In understanding these phenomena, it may be said that the wave-like picture of light of Maxwell revived rather than the corpuscular picture of photons of Einstein.

Y. Kayanuma (✉)
Laboratory for Materials and Structures, Tokyo Institute of Technology, Nagatsuta, Yokohama, Japan
e-mail: kayanuma.y.aa@m.titech.ac.jp

Department of Physical Sciences, Osaka Prefecture University, Sakai, Osaka, Japan

41

The primary interest is in the phenomena of photo-ionization by a long wavelength but intense light field. In this connection, one of the surprising achievements in this decade is the demonstration of carrier multiplication in semiconductors by terahertz pulses with magnitude of 1–MVcm^{-1} [1]. Such an excitation of electrons to the higher excited states may induce further extraordinary dynamical processes. For the salient examples in this category, we may name the phenomena called the high harmonic generation (HHG) from the strongly laser-driven atoms [2] and solids [3].

These developments in experimental physics require novel theoretical frameworks to treat such a highly nonlinear interactions of light and matter non-perturbatively. Since the pioneering work by Keldysh [4], a number of elaborate theories have been proposed on this subject, both in the atoms and molecules [5–8] and in solids [9, 10]. As noticed by Becker and Faisa [11], the highly nolinear electron dynamics in the intense fields can be formulated as a quest for the scattering matrix. An important point in calculating the scattering matrix is that the equation of motion for a free electron in the arbitrary time-dependent electric field has already been solved. The eigen state is called a Volkov state [12] in the free vacuum, and a Houston state [13] in the periodic lattice structure.

In the present article, I would like to add yet another contribution to this subject. In our approach, we formulate the time-dependent problem in the form of an integral equation of Volterra-type, where the integral kernel is explicitly obtained using the Houston state representation. Although this is equivalent to the numerical solution of the Schrödinger's differential equation, it has some advantages over the differential equation.

For the purpose of demonstration, I take two examples of application, the problem of population inversion in air-lasing, and the HHG in solids. These examples represent two typical situations of the spatial extension of light-matter interaction. In the first example, the optical transition is localized at the position of the molecule. In the case of HHG in solids, the transtion occurs throughout the bulk crystal from the valence band to the conduction band according to the translational symmetry of the crystal lattice. It will be be shown that, in both cases, a closed expression for the optical responses is obtained.

3.2 Population Inversion in N_2^+ Ions in the Intense Laser Beam

It is well known that, when an intense light beam passes through a transparent medium, say air, self focusing and filamentation of the beam often occur due to the nonlinear optical effects [14]. Sometimes this was a nuisance for experimentalists. Since the advent of high intensity ultrashort lase pulses, a possibility of application of this phenomenon emerged. The filaments in air are often accompanied with luminescence or even lasing to forward or backward [15] of the pumping beams. The spectrum of backward scattered fluorescence or lasing will be a source of remote sensing. In

the case of N_2 molecules in air, the forward lasing is the dominant pathway and the backward lasing is reported to be observed only under limited conditions [16]. In the ambient conditions of the air, the backward lasing is strongly depressed by the presence of oxygen molecules.

For the origin of lasing at 391.4 nm (3.17 eV) emission from N_2, a widely accepted view is that it is mainly due to the induced emission from the excited state of N_2^+ ions, mostly assigned to $B^2\Sigma_u^+ \rightarrow X^2\Sigma_g^+$ [15, 17]. The lasing of air can be initiated by the irradiation of fundamentals of Ti-sapphire laser. The photon energy (1.55 eV)is far below the ionization energy of N_2 (16 eV). Therefore, at least two question must be answered: What is the mechanism of ionization by below-threshold excitation? What is the mechanism of population inversion in the N_2^+ ions?

Population inversion in N_2^+ ions is a little surprising, because if the transition from the ground state to the excited state within the N_2 molecule occurs first, the photo-ionization from the excited state will follow much faster than that from the Σ_g state. In [18], the authors considered that the population inversion occurs within a single pump pulse in the reversed order. In the first half of the pulse, an electron of the highest occupied molecular orbital (HOMO) in a neutral N_2 molecule is ejected to the free state. Then the electronic configuration changes suddenly due to the transition $N_2 \rightarrow N_2^+$: The second ionization potential becomes much larger, while the excitation energy to the lowest unoccupied molecular orbital (denoted as B) becomes lower. An electron in the HOMO (denoted as X) of N_2^+ is excited to the B state by the electric field in the last half of the pulse. The abrupt emergence of the new electronic configuration gives rise to the double excitation as a highly nonadiabatic process. The authors carried out a simulation of the population change in a simple model within the assumption that a two-level system in the ground state is suddenly put in the intense off-resonant field at the moment of maximum intensity. Although it is noticed that the couplings between other excited states also plays a role [19–21], the essential mechanism would be the same.

In the following section, I would like to examine this model of air lasing by a simulation on a toy model with a very simple calculation. In order to mimic the ultrafast electron dynamics for a molecule in vacuum, we introduce a discrete structure into the vacuum with a small mesh of a nearest neighbor hopping. The quantum mechanical equation of motion for the ejected electron is then described by a tight-binding model, and the bound states of molecule are replaced by localized states in the lattice. This model is originally considered for the ultrafast electron dynamics in the crystals. For the technique of solving the Schrödinger equation, a method of Volterra integral equation of second kind [22, 23] is proposed. The advantage of this method is its simplicity and flexibility for the extension taking into account various effects.

A. **Volterra Integral Equation**

Let us assume a simple cubic "crystal structure" in three dimensions with the lattice constant a and hopping parameter $-B/2$. Furthermore, an additional site or "impurity state" is assumed at the origin. The Hamiltonian for the tight binding model in this space is written as

$$H_0 = -\frac{B}{2} \sum_{\alpha=x,y,z} \sum_{j_\alpha}' (|j_\alpha + 1\rangle\langle j_\alpha| + H.c.) + \epsilon_c \sum_{j_x, j_y, j_z} |j_x, j_y, j_z\rangle\langle j_x, j_y, j_z| + \epsilon_0 |g\rangle\langle g|.$$

$$(3.1)$$

In the above equation, $|j_x, j_y, j_z\rangle = |j_x\rangle \otimes |j_y\rangle \otimes |j_z\rangle$ means the state vector at the site index (j_x, j_y, j_z), where $\otimes$ is the direct product. The symbol $\sum_{j_\alpha}'$ means that the index j_α runs over N sites $j_\alpha = -\frac{N}{2}, -\frac{N}{2} + 1, \ldots, 0, \ldots, \frac{N}{2} - 2, \frac{N}{2} - 1$ with N being a very large even number. The Symbol $\sum_{j_\alpha}$ indicates the sum over $N + 1$ site from $-N/2$ to $N/2$. The state vector $|g\rangle$ is the "impurity state" located at $(0, 0, 0)$ site with the energy $\epsilon_0(= 0)$ chosen as the origin of the energy. The band-center energy is denoted as ϵ_c.

The eigenstate of H_0 in the conduction band is written as $|k_x, k_y, k_z\rangle = |k_x\rangle \otimes |k_y\rangle \otimes |k_z\rangle$ where

$$|k_\alpha\rangle = 1/\sqrt{N} \sum_{j_\alpha} |j_\alpha\rangle \exp[iak_\alpha j_\alpha], \qquad -\pi/a \le k_\alpha \le \pi/a \quad (\alpha = x, y, z),$$

$$(3.2)$$

with the eigenvalue

$$\epsilon_{k_x, k_y, k_z} = \epsilon_c - B\left(\cos k_x a + \cos k_y a + \cos k_z a\right), \qquad -\pi/a \le k_\alpha \le \pi/a. \quad (3.3)$$

Hereafter, we use the convention $\vec{k} = (k_x, k_y, k_z)$ and $\vec{j} = (j_x, j_y, j_z)$.

The low energy states in the conduction band of the tight binding model can be regarded as describing the free states in vacuum. In fact, in the limit $|k_\alpha a| << 1$, the above equation can be approximated as

$$\epsilon_{\vec{k}} \simeq \epsilon_c - 3B + \frac{Ba^2}{2}\vec{k}^2. \qquad (3.4)$$

Comparing this with the energy of a free electron in vacuum, $\epsilon_{\vec{k}} = \hbar^2\vec{k}^2/2m$, where m is the mass of electron, we find $m = \hbar^2/Ba^2$. In the case of N_2 molecule in vacuum, $|g\rangle$ corresponds to the HOMO, and $\epsilon_c - 3B$ is the ionization energy ($\simeq 16$ eV).

We assume that a linearly polarized pump pulse with polarization in the x-direction hits the sample along the z-axis. The interaction with the intense electromagnetic field will induce two kind of action on the initially localized electrons. The one is the excitation of the localized electron to the continuum state. This effect will be called an *inter-band driving*. The second is the perturbation of the excited states due to the optical Stark effect, which will be called an *intra-band driving*.

The Hamiltonian for the intra-band driving is written as

$$H_1(t) = -eaE(t) \sum_{j_x} j_x |j_x\rangle\langle j_x|, \qquad (3.5)$$

where $E(t)$ is the electric field of the laser pulse. The Hamiltonian for the inter-band driving is given by

Fig. 3.1 Image of portal
state
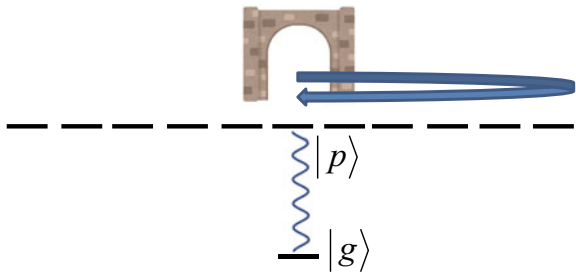
$$H_2(t) = E(t) \sum_k \left(\mu_k |k\rangle\langle g| + \mu_k^* |g\rangle\langle k| \right), \tag{3.6}$$

where μ_k is the transition dipole moment of the HOMO or impurity state to the state $|k\rangle$ in the conduction band defined in the length gauge as

$$\mu_k = -\langle k|er|g\rangle,$$

with $-er$ being the dipole moment of the molecule ($e > 0$). For the electric field of the pump-pulse, we assume the Gaussian form,

$$E(t) = E_0 \exp[-t^2/\sigma^2] \cos(\omega t + \varphi), \tag{3.7}$$

where σ is the pulse-width and φ is the carrier-envelope phase (CEP). For the pulse-width not extremely short, the CEP-dependence of the responses is negligible. Therefore, we set $\varphi = 0$ in the present work. We assumed an x-polarized light hits the material along the z-direction. The theory can be readily extended to the circularly polarized light.

It is noticeable that $H_2(t)$ is written as

$$H_2(t) = \mu E(t) \big(|p\rangle\langle g| + |g\rangle\langle p| \big), \tag{3.8}$$

where $|p\rangle$ is given by

$$|p\rangle = \mu^{-1} \sum_k \mu_k |k\rangle, \tag{3.9}$$

with $\mu = \sqrt{\sum_k |\mu_k|^2}$. We call $|p\rangle$ a *portal state* because the electron goes out from or comes back to the ground state $|g\rangle$ only through $|p\rangle$ as shown in Fig. 3.1.

The portal state is a localized state around $|g\rangle$ with spatial extension of the same order of $|g\rangle$. The actual functional form of $|p\rangle$ is given once the transition dipole moment μ_k is given. Although the following theory can be constructed for a general case of $|p\rangle$, we assume here, for simplicity, that $|g\rangle$ is well localized at the origin, so that μ_k is approximately independent of k. Then, $|p\rangle$ is given by the state $|0, 0, 0\rangle$ in the site-representation. In other words, we assume a vertical transition in real space.

At this point, a comment may be in order on the analogy and difference between the electron dynamics in solids and in true vacuum. In solids, Bloch's theory tells that the electronic states are described by linear combinations of the atomic like localized states (Wannier states). The magnitude and the selection rule for optical transitions are determined, roughly speaking, by the Wannier functions and the overlapping of the envelope functions. In the present article, the state $|k\rangle$ represents the envelope functions of the Bloch states, with atomic functions being implicitly accompanied. In the case of electrons in real vacuum, $|k\rangle$ should be a plane wave state or a scattering state.

Now we calculate the time-resolved photo-ionization probability of the localized electron with the integral equation method. For that purpose, the intra-band driving term $H_1(t)$ is included into an unperturbed Hamiltonian with definition,

$$\tilde{H}_0(t) \equiv H_0 + H_1(t).$$

The Schrödinger equation for the state vector $|\psi(t)\rangle$,

$$i\hbar \frac{d}{dt}|\psi(t)\rangle = \left\{\tilde{H}_0(t) + H_2(t)\right\}|\psi(t)\rangle \tag{3.10}$$

is transformed into an integral equation,

$$|\psi(t)\rangle = -(i/\hbar) \int_{-\infty}^{t} \exp_+\left[-(i/\hbar)\int_{\tau}^{t} \tilde{H}_0(\tau')d\tau'\right] H_2(\tau)|\psi(\tau)\rangle d\tau$$

$$+ \exp_+\left[-(i/\hbar)\int_{-\infty}^{t} \tilde{H}_0(\tau)d\tau\right]|g\rangle, \tag{3.11}$$

where $\exp_+$ is the time-ordered exponential, and $|g\rangle$ is the initial state at $t = -\infty$. The proof of (3.11) can be easily done by differentiating both sides of (3.11) with respect to t, and show that it is equivalent to (3.10).

We calculate the probability amplitudes $C_p(t)$ and $C_g(t)$ that the electron is found at the portal state $C_p(t) = \langle p|\psi(t)\rangle$, and at the ground state $C_g(t) = \langle g|\psi(t)\rangle$ at time t. From (3.11), we find a pair of integral equations,

$$C_p(t) = -(i/\hbar) \int_{-\infty}^{t} \langle p|\exp_+\left[-(i/\hbar)\int_{\tau}^{t} \tilde{H}_0(\tau')d\tau'\right]|p\rangle \mu E(\tau)C_g(\tau)d\tau, \tag{3.12}$$

$$C_g(t) = -(i/\hbar) \int_{-\infty}^{t} \mu E(\tau)C_p(\tau)d\tau + 1. \tag{3.13}$$

In (3.12), the integral kernel

$$K_{p,p}(t, \tau) \equiv \langle p| \exp_+\left[-(i/\hbar)\int_\tau^t \tilde{H}_0(\tau')d\tau'\right]|p\rangle$$

can be calculated analytically in the limit $N \to \infty$. This is because the Hamiltonian $\tilde{H}_0(t)$ is a sum of independent terms in the x, y and z direction. We find

$$K_{p,p}(t, \tau) = e^{-(i/\hbar)\epsilon_g(t-\tau)} K_0(t, \tau)^2 K_1(t, \tau), \qquad (3.14)$$

in which

$$K_0(t, \tau) = J_0(B|t - \tau|/\hbar), \qquad (3.15)$$

$$K_1(t, \tau) = J_0(B|R(t, \tau)|/\hbar), \qquad (3.16)$$

where $J_0(x)$ is the 0th order Bessel function, and $R(t, \tau)$ is given by the Lie algebraic argument [24] as

$$R(t, \tau) = \int_\tau^t \exp\left[-i(ea/\hbar)\int_\tau^u E(s)ds\right]du. \qquad (3.17)$$

The numerical solution of the integral equations was done by discretizing the time into meshes with small intervals. The numerical integration is written as a summation using the trapezoidal approximation. This gives the iterative relations for the values $C_p(t)$ and $C_g(t)$ with those of former time-bin, and determined successively.

In the two types of kernels, $K_0(t, \tau)$ represents the quantum diffusion to y, and z direction. The kernel $K_1(t, \tau)$ represents the motion of the electron in the x direction under the influence of the oscillating electric field. It is noticed that this intra-band driving term is important in the below threshold photo ionization because it induces the tunneling excitation as schematically shown in Fig. 3.2. However, it is found that, at least within the present model calculation, the effect of this term becomes significant only for a one-dimensional model. In three-dimension, the photo ionization probability becomes enhanced appreciably only for very high intensities of the electric field. This term is extremely important for the process of the high harmonic generation. The existence of the long plateau in the HHG spectrum is solely attributed to the intra-band driving as shown later.

B. **Application to Population Inversion**

Zhang and coauthors [18] studied theoretically their conjecture on the fundamental mechanism of population inversion in N_2 molecules under intense pulse irradiation by a simple two-level model. They calculated the probability of excitation of a two-level system after the passage of a modified Gaussian pulse. The temporal shape of
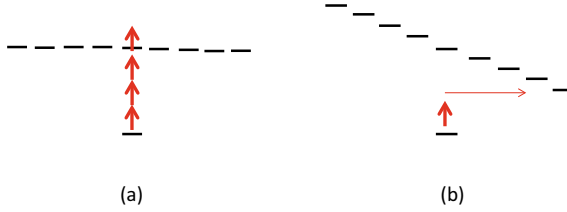
Fig. 3.2 Schematic picture for **a** the multi-photon excitation where the intra-band driving is absent, and **b** the tunneling excitation where the intra-band driving exists and plays an important role. Quantitatively, this effect is important for one-dimensional systems
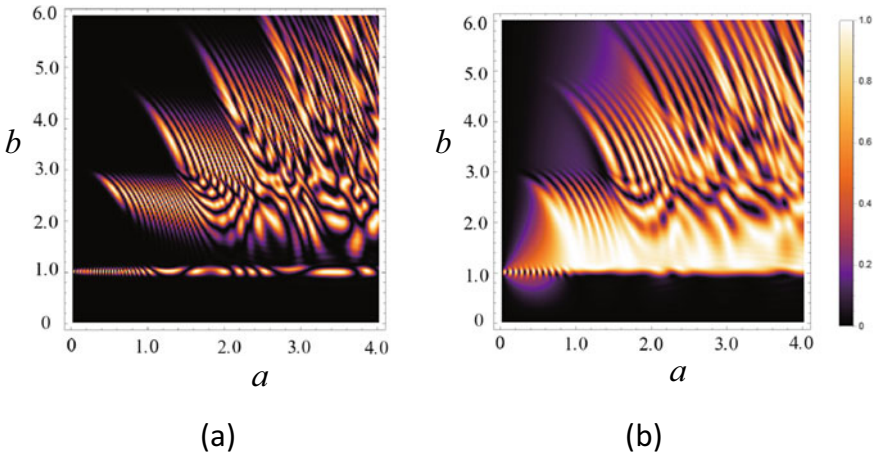

(a)   (b)

Fig. 3.3 Excitation probability of a two-level system plotted against the amplitude of the inter-band driving $a = \mu E_0/2\hbar\omega$ and the energy gap $b = \epsilon/\hbar\omega$. In **a**, the pump field is given by the Gaussian pulse $E(t) = E_0 e^{-t^2/\sigma^2} \cos\omega t$, and in **b** the pump field has a sudden rise as $E(t) = \theta(t)E_0 e^{-t^2/\sigma^2} \cos\omega t$ with $\theta(t)$ being the step function

the Gaussian pulse was strongly modified to a highly asymmetric form; the front half of the pulse has a sharp edge while the back half has an original Gaussian envelop. By the numerical simulation, they concluded that a necessary condition for the population inversion is the abrupt exposure to the intense optical field and the adiabatic fade away of the field strength.

In Fig. 3.3, the density plot of the excitation probability $P(a, b)$ in a two level system is shown in the two parameter space, $a = \mu E_0/2\hbar\omega$ and $b = \epsilon/\hbar\omega$, where ϵ is the energy difference of the two-level system. In Fig. 3.3a, $P(a, b)$ is shown for the original Gaussian pulse $E(t) = E_0 \exp[-t^2/\sigma^2] \cos(\omega t)$, while in (b), $P(a, b)$ is shown for the pulse shape $E(t) = \theta(t) E_0 \exp[-t^2/\sigma^2] \cos(\omega t)$, where $\theta(t)$ is a step function defined as $\theta(t) = 0$, for $t < 0$, and $\theta(t) = 1$ for $t \geq 0$. The pulse width is chosen as $\sigma = 20T$ where T is the oscillation period of the laser field. A part of Fig. 3.3b has been presented in [18].

Fig. 3.4 A proposed model of correlated electrons for the intense field induced population inversion in N_2 molecules
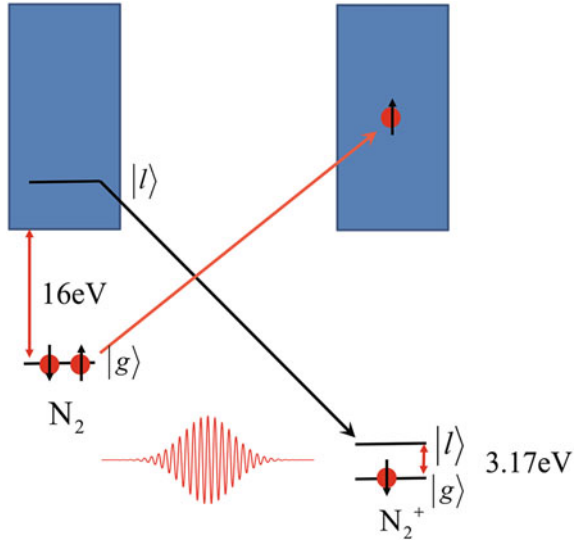
From Fig. 3.3, it is obvious that the highly asymmetric pulse with abrupt turning on and smooth fading away (Fig. 3.3b) is far more favorable for the population inversion than that with the normal Gaussian shape (Fig. 3.3a). Interestingly, a systematic and periodic pattern can be recognized in Fig. 3.3a. This may be explained by the adiabatic Floquet theory and path interference in the Landau-Zener transitions at quasi-level crossings [25]. In the plot Fig. 3.3b also, the periodic pattern in $P(a, b)$ is discernible.

In order to see the whole process in a unified way, we applied our calculation scheme to the population inversion in N_2 molecules in the intense pulse laser field. In Fig. 3.4, our model for the double excitation of N_2 molecules in the intense off-resonant pulse laser field is schematically shown. We assume two electrons are occupying the HOMO of N_2. For convenience, they are named "up-spin electron" and "down-spin electron", although the spin does not play any specific role in this problem. In the initial state, the on-site Coulomb energy U works like Hubbard model. The intense optical pulse first ejects one of the electrons, say, up-spin electron to the free state. Then the disappearance of U increases the second ionization energy. Furthermore, due to the incomplete screening of the core potential, the higher molecular orbital comes down, roughly to 3eV above the X-state of N_2^+, and prompts the excitation of the down-spin electron. Our purpose is to see the conditions for this scenario to work.

Our model Hamiltonian for the correlated two electrons is given as

$$H(t) = H_0(t) + H_I(t), \tag{3.18}$$

$$H_0(t) = \epsilon_g \left(u_g^\dagger u_g + d_g^\dagger d_g \right) + U u_g^\dagger u_g d_g^\dagger d_g + \left(\epsilon_l^0 + V u_g^\dagger u_g \right) d_l^\dagger d_l$$
$$+ \sum_k \epsilon_k u_k^\dagger u_k - ea E(t) \sum_{j_x} j_x u_{j_x}^\dagger u_{j_x}, \tag{3.19}$$

$$H_I(t) = E(t) \left(\mu_1 \sum_k \left(u_k^\dagger u_g + u_g^\dagger u_k \right) + \mu_2 \left(d_l^\dagger d_g + d_g^\dagger d_l \right) \right). \tag{3.20}$$

In the above equations, $d_g^\dagger$ and $d_l^\dagger$ are creation operators of the down-spin in the HOMO with energy ϵ_g and the lowest excited state with energy $\epsilon_l = \epsilon_l^0 + V u_g^\dagger u_g$, in which $u_g^\dagger$ and $u_k^\dagger$ are the creation operators of the up-spin state in the HOMO and the free state with energy ϵ_k, respectively. U and V are the on-site Coulomb energies between the up-spin electron and the down-spin electron. The electric field $E(t)$ is assumed to be an x-polarized pulse with functional form given in (3.7). The transition dipole moments from the HOMO are denoted μ_1 for the free state and μ_2 for the first excited state, respectively. In actual simulations, we set $\mu_1 = \mu_2 = \mu$, for simplicity. Note that our Hamiltonian (3.19) contains the Hamiltonians (3.1), (3.5), and (3.6) in the part of up-spin variables.

Although it is possible to solve the two-electron dynamics described by the above Hamiltonian, only an approximate solution is shown here. The up-spin electron plays a key role to control the whole ultra fast process by changing the energy levels for the down-spin electron. Therefore, we neglect the back-reaction from the down-spin electron to the up-spin electron. Note that we only name the electron that was ejected to continuum an up-spin electron, and that excited to the LUMO a down-spin electron. The actual numerical calculation was done as follows. First, the time-dependent probability of photo-ionization of the up-spin electron was calculated. This gives the population probability to the HOMO $n_\uparrow(t) = \langle u_g^\dagger u_g \rangle$. The energy of the first excited state ϵ_l is then evaluated as $\epsilon_l(t) = \epsilon_l^0 + V n_\uparrow(t)$. The transition dynamics for the down-spin is simultaneously calculated by solving the Schrödinger equation numerically for the two-level system $|g\rangle = d_g^\dagger |0\rangle$ and $|l\rangle = d_l^\dagger |0\rangle$, with input of the value $\epsilon_l(t)$. The on-site Coulomb energy U is roughly equal to the difference between the first and the second ionization energy of N_2, and V is set to be $18\hbar\omega$ in the numerical calculation.

In Fig. 3.5, two examples of the pulse-induced population inversion are plotted for the one-dimensional model. In Fig. 3.5a, b, the field strength is set to be $\mu E_0/\hbar\omega = ea E_0/\hbar\omega = 6.0$. In (a), the population of the up-spin electron to the HOMO of N_2 is plotted as a function of t, and in (b), the population of the down-spin electron to the B-state of N_2^+ is shown. In this case, the up-spin electron is almost completely ejected to the free state before the peak value of the pulse with half width $\sigma = 10T$. The down-spin electron undergoes a nonadiabatic transition to the B-state with a violent oscillation and smooth adiabatic convergence. In Fig. 3.5c, d, on the other hand, the field strength is set to be slightly lower, $\mu E_0/\hbar\omega = ea E_0/\hbar\omega = 5.9$. The probability of photo-ionization of the up-spin electron is almost complete as shown in (c). However, the population inversion of the down-spin electron is not attained as seen in (d). Detailed inspection into the power dependence of the final transition
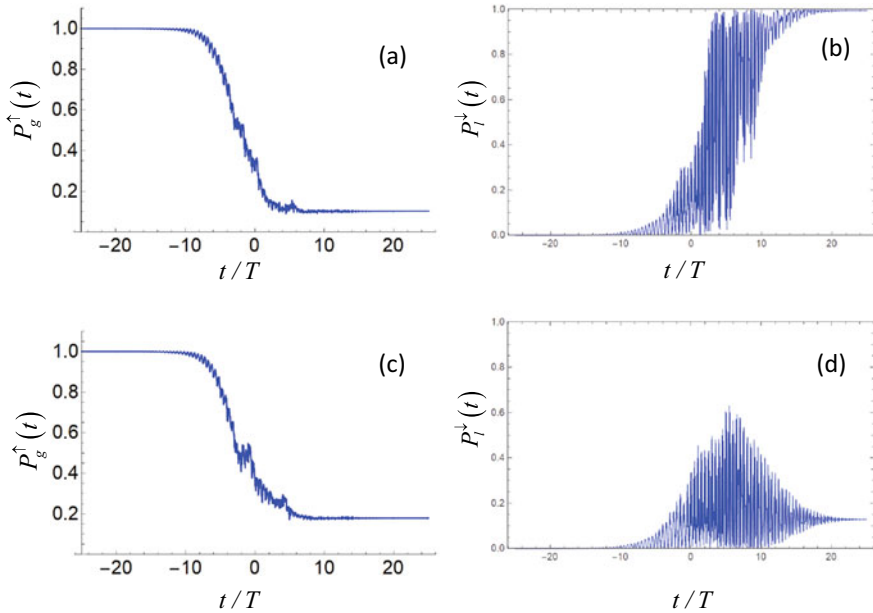
Fig. 3.5 The pulse-intensity dependence of the population change in the lowest excited state of N_2^+ ions. **a** The population to the highest occupied state of the up-spin electron of N_2 molecule, for $\mu E_0/\hbar\omega = eaE_0/\hbar\omega = 6.0$ and **b** the corresponding population to the lowest excited state of the down-spin electron. **c** The same as (**a**) with $\mu E_0/\hbar\omega = eaE_0/\hbar\omega = 5.9$ and **d** the corresponding population to the lowest excited state of the down-spin electron. Other parameter values are common to all of the figures, $B/\hbar\omega = 25$, $\epsilon_g/\hbar\omega = 35$, $\sigma/T = 10$

rate of the down-spin electron indicates that it is not a monotonic function of E_0 as can be expected from Fig. 3.3b.

3.3 High Harmonic Generations in Solids

Now, we extend the formalism developed in previous sections to the case of bulk solids in the intense pulse fields. A number of recent topics in the laser science can be classified in this category. Our interest is focused mainly on the above band-gap excitation of valence electrons in insulators, and subsequent high harmonic radiation. This subject has been attracting intense interest both of the experimentalists and theoreticians since the first report of HHG in solids [3]. For reviews on HHG in atoms and molecules in gas phase, see [26, 27] for example.

Following the success of the explanation of the HHG profile for the gas phase by a simple semi-classical model of Corkum [28] and its quantum mechanical version [29], a number of theories have been proposed for the HHG in solids. They may

be classified according to the methodology in the treatment of the interaction with an intense driving field in solids as the semiclassical one [30], semiconductor Bloch equation [31, 32], Floquet theory [33, 34], and so forth. Our purpose here is not to present a comprehensive review of these works, nor a detailed theoretical analysis of the experimental data, but to propose a new theoretical framework to overview this subject, based on a model as simple as possible.

A. **Crystal model of Two-Level Atoms**

Let us assume a simple cubic crystal of $N \times N \times N$ sites ($N >> 1$). Each site is occupied by a single atom with atomic orbitals, or Wannier functions, ϕ_c and ϕ_v. The energy difference between ϕ_c and ϕ_v is ϵ_c. Both of the ϕ_c and ϕ_v are coupled to the same kind of orbitals at the nearest neighbor atoms with the hopping parameters, $-B_c/2$ and $B_v/2$, respectively. This forms the conduction band and the valence band. This is the simplest toy-model of the band structure of a crystal lattice. The extension to a little more realistic model can be done, for example, by putting an s-orbital and three-fold degenerate p-orbitals at each site. This is the tight-binding model describing the band structures of carbon materials like graphene [35], or III-V semiconductors like GaAs [36].

Each site is designated with three indices j_x, j_y, j_z as before, and the indices c and v which designate the conduction and the valence band. The unperturbed Hamiltonian H_0 in this section is given by

$$
H_0 = -\frac{B_c}{2} \sum_{\alpha=x,y,z} \sideset{}{'}\sum_{j_\alpha} (|j_\alpha + 1, c\rangle\langle j_\alpha, c| + H.c.) + \epsilon_0 \sum_{\vec{j}} |\vec{j}, c\rangle\langle\vec{j}, c|
$$

$$
+ \frac{B_v}{2} \sum_{\alpha=x,y,z} \sideset{}{'}\sum_{j_\alpha} (|j_\alpha + 1, v\rangle\langle j_\alpha, v| + H.c.) , \tag{3.21}
$$

where the convention of the summation is the same as before. The Hamiltonian H_0 can be diagonalized by introducing the Bloch states $|\vec{k}, c\rangle$ and $|\vec{k}, v\rangle$,

$$
H_0 = \sum_{\vec{k}} \epsilon_c(\vec{k})|\vec{k}, c\rangle\langle\vec{k}, c| + \sum_{\vec{k}} \epsilon_v(\vec{k})|\vec{k}, v\rangle\langle\vec{k}, v|,
$$

where

$$
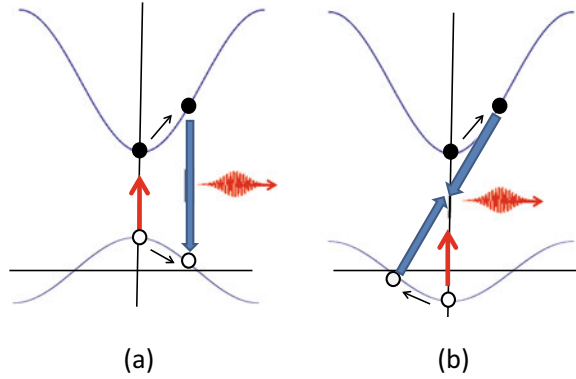\epsilon_c(\vec{k}) = \epsilon_0 - B_c \left(\cos k_x a + \cos k_y a + \cos k_z a\right),
$$

and

$$
\epsilon_v(\vec{k}) = B_v \left(\cos k_x a + \cos k_y a + \cos k_z a\right).
$$

The half-width of the conduction band and the valence band are $3B_c$ and $3B_v$, respectively. It is assumed that the band-gap $\epsilon_0 - 3(B_c + B_v)$ is much larger than the photon energy $\hbar\omega$.

Fig. 3.6 Schematic picture of the recombination luminescence in **a** electron-vacancy picture and **b** electron-hole picture.

(a)   (b)

The electromagnetic field of the optical pulse is assumed to be linearly polarized in the x-direction. The interaction with the electron can be divided into two as before. The intra-band driving term is given by

$$H_1(t) = -eaE(t) \sum_{j_x} j_x \left(|j_x, c\rangle\langle j_x, c| + |j_x, v\rangle\langle j_x, v| \right), \tag{3.22}$$

and the inter-band driving is by

$$H_2(t) = \mu E(t) \sum_{j_\alpha = x, y, z} \left(|j_\alpha, c\rangle\langle j_\alpha, v| + H.c. \right), \tag{3.23}$$

where the functional form of $E(t)$ is the same as (3.7).

In Fig. 3.6, the optical pumping and HHG process in our model is schematically depicted. In Fig. 3.6a, the electron in the conduction band, and a "vacancy" of electron in the valence band are shown by a solid circle, and an open circle, respectively. This vacancy should not be confused with the so called "hole" in the high-energy physicist's sense. The vacancy has a positive charge and negative mass at the zone center, so that it is accelerated in the k-space to the same direction as the electron. The hole is defined as a quasi particle which has a positive charge and positive mass at zone center. Furthermore, it has an opposite momentum and inversed value of energy to the vacancy as shown in (b). In Fig. 3.6a, the radiative recombination process of an electron-vacancy pair is schematically shown. In this view, the radiative recombination process is described as the vertical transition in the Bloch space. In Fig. 3.6b, the same process is shown in the electron-hole picture. In this view, the recombination process is described as a radiative pair annihilation of an electron and a hole with opposite momentum. The electron-vacancy view is common in the society of solid state physics, while the electron-hole picture, or particle-anti particle picture, is common among the high-energy physicists.

Hereafter, we adopt the electron-hole picture, because it is more suitable to describe the two-particle dynamics. The Hamiltonians (3.19)–(3.23) are written in the second quantized form as

$$H_0 = -\frac{B_c}{2} \sum_{\alpha=x,y,z} \sideset{}{'}\sum_{j_\alpha} \left(a^\dagger_{j_\alpha+1} a_{j_\alpha} + H.c. \right) + \sum_{\vec{j}} \epsilon_0 a^\dagger_{\vec{j}} a_{\vec{j}}$$

$$-\frac{B_v}{2} \sum_{\alpha} \sideset{}{'}\sum_{j_\alpha} \left(b^\dagger_{j_\alpha+1} b_{j_\alpha} + H.c. \right), \tag{3.24}$$

$$H_1(t) = -eaE(t) \sum_{j_x} j_x \left(a^\dagger_{j_x} a_{j_x} - b^\dagger_{j_x} b_{j_x} \right), \tag{3.25}$$

$$H_2(t) = \mu E(t) \sum_{\vec{j}} \left(a^\dagger_{\vec{j}} b^\dagger_{\vec{j}} + a_{\vec{j}} b_{\vec{j}} \right), \tag{3.26}$$

where $a^\dagger_{\vec{j}}$ and $b^\dagger_{\vec{j}}$ are creation operators for electron, and hole at $\vec{j}$th site, respectively, and the origin of energy is chosen at the vacuum of electrons and holes. It should be noted that the creation operators $a^\dagger_{\vec{j}}$ are defined as the direct product, $a^\dagger_{\vec{j}} = a^{x\,\dagger}_{j_x} \otimes a^{y\,\dagger}_{j_y} \otimes a^{z\,\dagger}_{j_z}$.

With the Fourier transformation,

$$a^\dagger_{\vec{j}} = \frac{1}{\sqrt{N^3}} \sum_{\vec{k}} a^\dagger_{\vec{k}} e^{-ia\vec{k}\vec{j}}, \quad b^\dagger_{\vec{j}} = \frac{1}{\sqrt{N^3}} \sum_{\vec{k}} b^\dagger_{\vec{k}} e^{-ia\vec{k}\vec{j}},$$
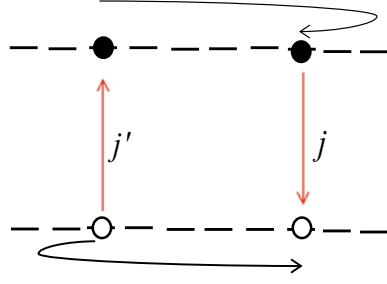
H_0 and $H_2(t)$ are rewritten as

$$H_0 = \sum_{\vec{k}} \left(\epsilon^c_{\vec{k}} a^\dagger_{\vec{k}} a_{\vec{k}} - \epsilon^v_{-\vec{k}} b^\dagger_{\vec{k}} b_{\vec{k}} \right), \tag{3.27}$$

$$H_2(t) = \mu E(t) \sum_{\vec{k}} \left(a^\dagger_{\vec{k}} b^\dagger_{-\vec{k}} + a_{\vec{k}} b_{-\vec{k}} \right), \tag{3.28}$$

which explicitly indicate the mechanism of generation of high energy photons by pair annihilations of an electron and a hole with opposite momentums, $\hbar\vec{k}$ and $-\hbar\vec{k}$ to yield a photon with zero momentum and energy $\epsilon^c_{\vec{k}} + \left(-\epsilon^v_{-\vec{k}} \right)$ as shown in Fig. 3.7.

B. **Calculation of HHG Probability**

Now we calculate the probability of HHG within the framework of the integral
equation. For that purpose, the intra-band driving term $H_1(t)$ is included into an
unperturbed Hamiltonian with definition,

$$\tilde{H}_0(t) \equiv H_0 + H_1(t),$$
$$= H_0^c(t) + H_0^v(t), \tag{3.29}$$

with

$$H_0^c(t) = \sum_{\vec{k}} \epsilon_{\vec{k}}^c a_{\vec{k}}^\dagger a_{\vec{k}} - eaE(t) \sum_{j_x} j_x a_{j_x}^\dagger a_{j_x},$$

$$H_0^v(t) = -\sum_{\vec{k}} \epsilon_{-\vec{k}}^v b_{\vec{k}}^\dagger b_{\vec{k}} + eaE(t) \sum_{j_x} j_x b_{j_x}^\dagger b_{j_x}. \tag{3.30}$$

The Schrödinger equation for the state vector $|\psi(t)\rangle$,

$$i\hbar \frac{d}{dt} |\psi(t)\rangle = \left\{ \tilde{H}_0(t) + H_2(t) \right\} |\psi(t)\rangle \tag{3.31}$$

is transformed into an integral equation,

$$|\psi(t)\rangle = -(i/\hbar) \int_{-\infty}^{t} \exp\left[-(i/\hbar) \int_{\tau}^{t} \tilde{H}_0(\tau')d\tau' \right] H_2(\tau)|\psi(\tau)\rangle d\tau$$

$$+ \exp\left[-(i/\hbar) \int_{-\infty}^{t} \tilde{H}_0(\tau)d\tau \right] |\psi_g\rangle, \tag{3.32}$$

where $|\psi_g\rangle$ is the initial state at $t = -\infty$ and is given by the vacuum of electron and
hole, $|\psi_g\rangle = |0\rangle$. We calculate the probability amplitude $C_{\vec{j}}(t) \equiv \langle 0|a_{\vec{j}} b_{\vec{j}}|\psi(t)\rangle$ that
the electron and the hole are found at $\vec{j}$th site at time t. It should be noted that the

electron and the hole are always created at the same site, but once created, they are driven in the conduction band and the valence band independently, until they collide at another identical site and are annihilated simultaneously.

We adopt here a single-pair approximation, in which the simultaneous excitations of multiple electron-hole pairs are neglected. This is justified if the energy gap is large enough, and if the electromagnetic field is not extremely intense. Within this approximation the amplitude $C_{\vec{j}}(t)$ is calculated from (3.11) and (3.13) as

$$
C_{\vec{j}}(t) = -(i/\hbar) \sum_{\vec{j}'} \int_{-\infty}^{t} \langle 0|a_{\vec{j}} \exp[-(i/\hbar) \int_{\tau}^{t} H_0^c(\tau')d\tau']a_{\vec{j}'}^{\dagger}|0\rangle
$$

$$
\times \langle 0|b_{\vec{j}} \exp[-(i/\hbar) \int_{\tau}^{t} H_0^v(\tau')d\tau']b_{\vec{j}'}^{\dagger}|0\rangle \langle 0|\psi(\tau)\rangle \mu E(\tau)d\tau. \quad (3.33)
$$

For the amplitude in the ground state $C_g(t) \equiv \langle 0|\psi(t)\rangle$, we find

$$
C_g(t) = -(i/\hbar) \sum_{\vec{j}} \int_{-\infty}^{t} C_{\vec{j}}(\tau)\mu E(\tau)d\tau + 1. \quad (3.34)
$$

If we define the kernels for the electron,

$$
K_{\vec{j},\vec{j}'}^{(c)}(t, \tau) \equiv \langle 0|a_{\vec{j}} \exp[-(i/\hbar) \int_{\tau}^{t} H_0^c(t')d\tau']a_{\vec{j}'}^{\dagger}|0\rangle
$$

and for the hole,

$$
K_{\vec{j},\vec{j}'}^{(v)}(t, \tau) \equiv \langle 0|b_{\vec{j}} \exp[-(i/\hbar) \int_{\tau}^{t} H_0^v(t')d\tau']b_{\vec{j}'}^{\dagger}|0\rangle,
$$

the above equations are written as

$$
C_{\vec{j}}(t) = -(i/\hbar) \sum_{\vec{j}'} \int_{-\infty}^{t} K_{\vec{j},\vec{j}}^{(c)}(t, \tau) K_{\vec{j},\vec{j}}^{(v)}(t, \tau) C_g(\tau)\mu E(\tau)d\tau, \quad (3.35)
$$

$$
C_g(t) = -(i/\hbar) \sum_{\vec{j}} \int_{-\infty}^{t} C_{\vec{j}}(\tau)\mu E(\tau)d\tau + 1. \quad (3.36)
$$

The kernels $K^{(c)}_{\vec{j},\vec{j}'}(t,\tau)$ and $K^{(v)}_{\vec{j},\vec{j}'}(t,\tau)$ describe the transition amplitudes that the electron (hole) is found at the site $\vec{j}$ at time t under the condition it exists at the site $\vec{j}'$ at time τ with the influence of quantum hopping with uniform driving field. They can be obtained analytically as

$$K^{(c)}_{\vec{j},\vec{j}'} = e^{-(i/\hbar)\epsilon_0(t-\tau)} K^{(c)}_{j_x,j'_x}(t,\tau) K^{(c)}_{j_y,j'_y}(t,\tau) K^{(c)}_{j_z,j'_z}(t,\tau), \tag{3.37}$$

$$K^{(v)}_{\vec{j},\vec{j}'} = K^{(v)}_{j_x,j'_x}(t,\tau) K^{(v)}_{j_y,j'_y}(t,\tau) K^{(v)}_{j_z,j'_z}(t,\tau), \tag{3.38}$$

in which

$$K^{(c)}_{j_x,j'_x}(t,\tau) = \exp[i\frac{\pi}{2}(j_x - j'_x)] J_{j_x-j'_x}\left(B_c|R(t,\tau)|\right), \tag{3.39}$$

$$K^{(c)}_{j_y,j'_y}(t,\tau) = \exp[i\frac{\pi}{2}(j_y - j'_y)] J_{j_y-j'_y}\left(B_c|t-\tau|\right), \tag{3.40}$$

$$K^{(c)}_{j_z,j'_z}(t,\tau) = \exp[i\frac{\pi}{2}(j_z - j'_z)] J_{j_z-j'_z}\left(B_c|t-\tau|\right), \tag{3.41}$$

where $J_j(x)$ is jth order Bessel function, and $R(t,\tau)$ is given in (3.17). For the kernel of the hole, $K^{(v)}_{\vec{j},\vec{j}'}$, the analogous expressions to the above formula are obtained, with only difference that B_c must be replaced by B_v. Strictly speaking, the above formulas are derived for the infinitely large tight binding model, but it is approximately valid under the condition $N >> 1$. The fact that the integral kernels are completely decoupled into the three components of the direction of motion is an advantage of the present theory in the time domain. Furthermore, using Neumann's sum rule,

$$\sum_{n=-\infty}^{\infty} J_n(a) J_n(b) e^{in\theta} = J_0(\sqrt{a^2 + b^2 - 2ab \cos\theta}), \tag{3.42}$$

we can carry out the summation over the creation sites of the electron-hole pair, and finally obtain

$$C_{\vec{j}}(t) = -(i/\hbar) \int_{-\infty}^{t} e^{-(i/\hbar)\epsilon_g(t-\tau)} J_0\left((B_c + B_v)|R(t,\tau)|\right) \tag{3.43}$$

$$\times J_0\left((B_c + B_v)|t-\tau|\right)^2 C_g(\tau) \mu E(\tau) d\tau, \tag{3.44}$$

$$C_g(t) = -(i/\hbar) \sum_{\vec{j}} \int_{-\infty}^{t} C_{\vec{j}}(\tau) \mu E(\tau) d\tau + 1.$$

So far, we have not taken into account any relaxation phenomena in the dynamical processes. Furthermore, in actual experiments, the observed intensity of the high harmonics depends on the spot-size of the pump pulse. Therefore, we introduce here

the effective number of atoms N_{eff} that contribute to high harmonic generation. Since $C_{\vec{j}}(t)$ does not depend on $\vec{j}$, we may set $C_{\vec{j}}(t) = C_p(t)/\sqrt{N_{eff}}$, and find

$$C_p(t) = -(i/\hbar) \int_{-\infty}^{t} e^{-(i/\hbar)\epsilon_g(t-\tau)} J_0\left((B_c + B_v)|R(t,\tau)|\right) \times J_0\left((B_c + B_v)|t - \tau|\right)^2 C_g(\tau)\mu_{eff} E(\tau)d\tau, \quad (3.45)$$

$$C_g(t) = -(i/\hbar) \int_{-\infty}^{t} C_p(\tau)\mu_{eff} E(\tau)d\tau + 1. \quad (3.46)$$

where $\mu_{eff} = \sqrt{N_{eff}}\,\mu$ is the effective dipole moment.

For the source of harmonic radiation in solids, two mechanism of polarization can be considered. The one is the intra-band polarization, and the other is the inter-band polarization [37]. The electromagnetic radiation from the intra-band polarization is due to the non-parabolicity of the band dispersion. The inter-band polarization corresponds to the recombination emission. Numerical calculations show that the intra-band contribution is usually smaller than that of the inter-band one [30]. So, we consider only the contribution from the inter-band transition radiation here. The time-dependent amplitude of the emitted radiation $A(t)$ is proportional to the expectation value of the source term $\sum_{\vec{j}} a_{\vec{j}} b_{\vec{j}}$ as

$$A(t) = \langle \psi(t)| \sum_{\vec{j}} a_{\vec{j}} b_{\vec{j}} |\psi(t)\rangle. \quad (3.47)$$

Because the component of the excited states in $|\psi(t)\rangle$ is very small in the present parameter values, we can safely write

$$A(t) = \langle 0| \sum_{\vec{j}} a_{\vec{j}} b_{\vec{j}} |\psi(t)\rangle = \sum_{\vec{j}} C_{\vec{j}}(t).$$

The intensity of high harmonics photons of frequency Ω per unit density of atoms is then given by the Fourier transform of $C_p(t)$ as

$$I(\Omega) = \left| \int_{-\infty}^{\infty} C_p(t) \exp[i\Omega t]dt \right|^2. \quad (3.48)$$

It is remarkable that the above formulas (3.45) and (3.46) for the HHG in the bulk crystals are formally the same as the (3.12), (3.13), which are derived for the electron dynamics in the impurity state, or a molecule in the vacuum in the previous section. This suggests that the mechanism of the HHG in the crystal is essentially the same as that in a gas in vacuum. A difference is that the parameter for the half band-width in the latter model is the sum of B_c and B_v, in contrast to the former case, where only the half band-width B_c appears in the formula.
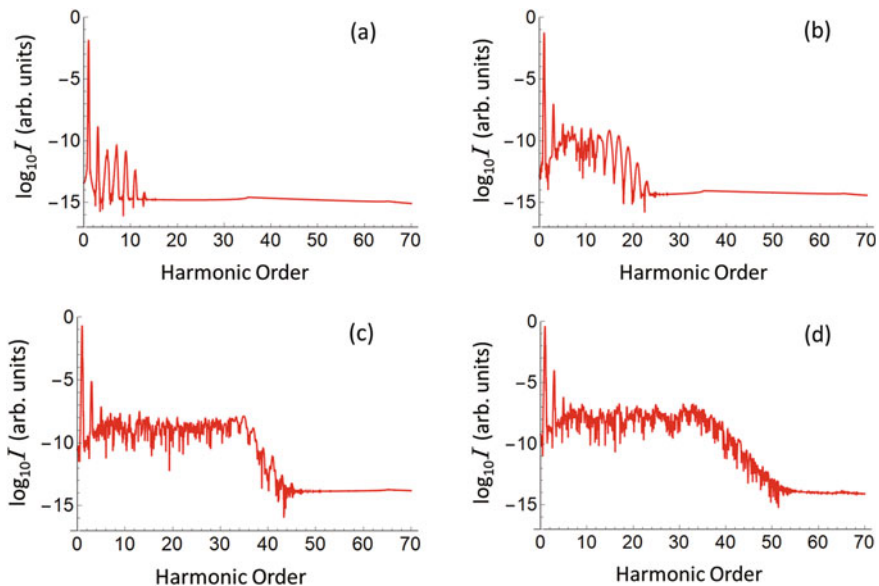
Fig. 3.8 Theoretical results for the high harmonic spectrum. The parameter values are $(B_c + B_v)/\hbar\omega = 15$, $\epsilon_g/\hbar\omega = 50$ which correspond to the band-gap $5\hbar\omega$, $\sigma = 5T$. The field intensities are **a** $eaE_0 = \mu_{eff}E_0 = 0.5\hbar\omega$, **b** $eaE_0 = \mu_{eff}E_0 = 1.0\hbar\omega$, **c** $eaE_0 = \mu_{eff}E_0 = 2.0\hbar\omega$, **d** $eaE_0 = \mu_{eff}E_0 = 3.0\hbar\omega$, respectively.

In Fig. 3.8, the dependence of the high harmonic spectra on the incident pulse-amplitude are shown for the three dimensional tight-binding model. The parameter values are $B_c + B_v = 15\hbar\omega$ (total half band-width= $45\hbar\omega$), $\epsilon_0 = 50\hbar\omega$ which corresponds to the band gap $5\hbar\omega$ at Γ-point. The incident pulse is linearly polarized in the x-direction, and the pulse-width is $\sigma = 5T$ where $T = 2\pi/\omega$. The amplitude of the electric field is chosen as (a) $eaE_0/\hbar\omega = \mu_{eff}E_0/\hbar\omega = 0.5$, (b) $eaE_0/\hbar\omega = \mu_{eff}E_0/\hbar\omega = 1.0$, (c) $eaE_0/\hbar\omega = \mu_{eff}E_0/\hbar\omega = 2.0$ and (d) $eaE_0/\hbar\omega = \mu_{eff}E_0/\hbar\omega = 3.0$.

The theoretical results in Fig. 3.8 reproduce the experimental features [3, 38] fairly well. The high harmonic spectrum has a long plateau and a sudden cutoff. Experimentally, it is observed that the spectrum obeys the optical selection rule that only the odd order harmonics have appreciable intensities for crystals with space-inversion symmetry. In the theoretical line shapes, however, such a selection rule seems to be blurred except for the low order harmonics and those near cutoff. This is paradoxical since the theoretical results derived on a simple symmetrical model gives much more noisy curves than the experimental data. The elucidation of this paradox has been attracting theoretical interest recently. It is reported that the selection rule is recovered [30, 39, 40] if one takes into account some mechanism of dephasing in his model. In a phenomenological model [30], it was shown that a surprisingly short dephasing time, as short as 1 femtosecond, is required in order to get agreement

Fig. 3.9 The dependence on
the intra-band driving of the
HHG spectrum for
$\mu_{eff}E_0/\hbar\omega = 1.0$ with **a**
$eaE_0 = 0$ and **b**
$eaE_0/\hbar\omega = 3.0$
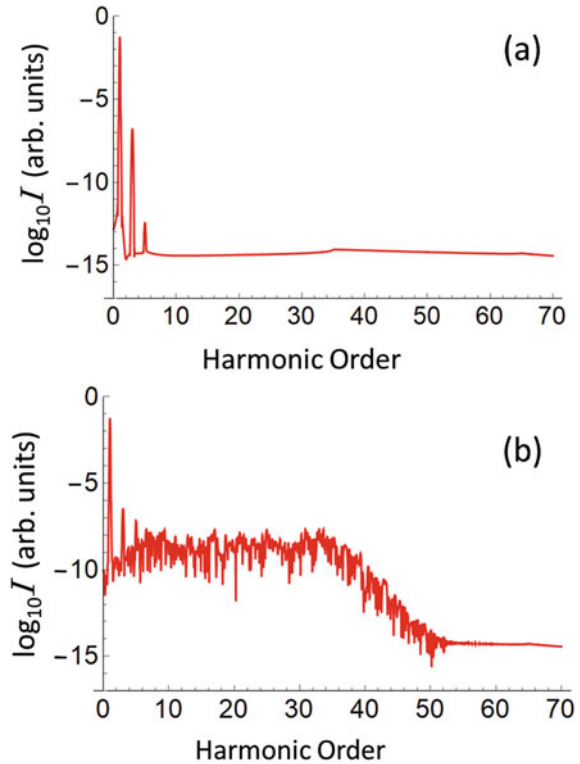
with experimental data. It was also asserted that the pulse propagation in the dense
and inhomogeneous media also plays a role to make the experimental HHG spectra
clean [41]. This is an intriguing open question.

In order to clarify the distinct roles of the inter-band driving and the intra-band
driving, the theoretical line shapes of the high harmonics are shown in Fig. 3.9 for
two set of parameter values, namely for $\mu_{eff}E_0 = 1.0$ and $eaE_0 = 0$ (no intra-band
driving) in (a) and $\mu_{eff}E_0 = 1.0$ and $eaE_0 = 3.0$ (strong intra-band driving) in (b).
In Fig. 3.9a, only the 1st, 3rd and 5th harmonics are seen. In contrast, a long plateau
of high harmonics is observed in Fig. 3.9b. Note that the line-shape is almost the same
as shown in Fig. 3.8d. This means that the total line-shape of the high harmonics is
entirely determined by the intra-band driving field, although its amplitude depends
on the inter-band driving.

The features in these line-shape of HHG qualitatively agree with those reported [3,
38] and with the simple formula of the three-step model [28]. Quantitatively, however,
the agreement with the formula by the three-step model in not good. The three-step
model predicts the energy of the cutoff of the plateau E_c as

$$E_c = I_p + 3U_p, \tag{3.49}$$

where I_p is the ionization energy and U_p is the ponderomotive energy, $U_p = e^2 E_0^2/4m\omega^2$. From (3.4), we may set $I_p = \epsilon_g - 3(B_c + B_v)$ and $m = \hbar^2/(B_c + B_v)a^2$. But this gives a too small value of E_c. The main reason of the disagreement is the breakdown of the effective mass approximation. In the present model of a two-level atom crystal, it is assumed that the transition dipole moment is a constant and the optical transition is allowed all over the first Brillouin zone vertically. Although the main contribution comes from the excitation around the Γ-point because the transition probability depends also on the energy gap, the contribution from other region will not be negligible. In the present model of cosine-band, the effective mass becomes much smaller and even formally be zero at the band-center. For a quantitative analysis of the HHG spectra in solids, information on the actual band structure will be needed.

On the other hand, it is reported experimentally that the high-energy cutoff in solids has a linear dependence on the amplitude of drive laser field [42]. This is in agreement with the present theoretical result shown in Fig. 3.8. It is noticed that, in the theory, the gap between the edge of the plateau and the cutoff is extended in the high intensity limit as shown in Fig. 3.8d. In order to clarify all these features, further investigation will be needed into the electron dynamics in solids induced by the high intensity pulse fields.

3.4 Conclusion and Prospect

I have proposed a simple formalism based on an integral equation of Volterra-type to calculate the electron dynamics driven by intense pulse fields. It is an analogy of the Dyson equation in time-domain, but has some advantages compared with other more elaborate methods. If the wave-length of the electromagnetic field is much larger than the atomic scales, as is usually the case, the integral kernel for the propagation of the electron in the free-space or in the crystal lattice structures can be analytically obtained. Because the integral kernels are exponential functions, it is easily extended to higher dimensions.

In this article, I have shown two examples for the application of this method. In the Section II, the electron is assumed to make transitions between a localized state and a delocalized "band". In the Section III, an electron and a hole make transitions between the two delocalized "bands" from the "vacuum". It is remarkable that the integral equations are reduced to a formally the same structure, if one introduces a "portal state". This suggests that the mechanism of the high harmonic generation in the system of atoms in vacuum and in the crystals are essentially the same. In the latter case, the translational symmetry plays an important role.

One of the difference in the two models treated here is the quantitative difference in the effective interaction amplitude with the external fields. In the case of crystals, the dipole moment for inter-band transition is enhanced by a factor $\sqrt{N_{eff}}$, where N_{eff} is the phenomenologically introduced effective number of atoms participating in the interaction with photons. The actual value of $\sqrt{N_{eff}}$ will be determined taking

into account the experimental conditions such as the spacial profile of the laser pulses, the relaxation times in the excited states and so forth. Anyway, it may be expected that the solids are promising candidate for the intense light source of high harmonics because of their higher atomic densities. Another difference of the electron dynamics in solids from that in vacuum is the existence of a periodic structure of lattice. Usually this is negligible in the low energy region. However, in the case of motion under the intense electromagnetic field, the discrete structure of the crystal lattice may become non-negligible. The criterion for this boundary is the ratio $aE_0/\hbar\omega$. In fact, in the simple tight-binding picture, the effective transfer energy B is reduced to zero for $aE_0/\hbar\omega = 2.405$ and even become negative i. e. the particle has a negative mass, for $2.405 < aE_0/\hbar\omega < 5.52$. This phenomenon is called a dynamic localization [43] or a band-collapsing [44]. This is due to the coherent path-interference [24] in the driven quantum system. This effect has been automatically incorporated in the expression of the integral kernels under uniform electromagnetic field. To the authors knowledge, clear experimental observation of the dynamic localization in real crystals is yet to be done. It may be a next target in the intense-laser science in solids.

References

1. H. Hirori, K. Shinokita, M. Shirai, S. Tani, K. Kadoya, K. Tanaka, Nat. Commun. **2**, 594 (2011)
2. C.-G. Wahlström, J. Larsson, A. Persson, T. Starczewski, S. Svanberg, P. Salieres, Ph Balcou, Anne L' Huillier. Phys. Rev. A **48**, 4709 (1993)
3. S. Ghimire, A.D. DiChiara, E. Sistrunk, P. Agostini, L.F. DiMauro, D.A. Reis, Nat. Phys. **7**, 138 (2011)
4. L.V. Keldysh, Sov. Phys. JETP **20**, 1307 (1965)
5. F.H.M. Faisal, J. Phys. B **6**, L89 (1973)
6. H.R. Reiss, Phys. Rev. A **22**, 1786 (1980)
7. K. Yabana, G.F. Bertch, Phys. Rev. B **54**, 4484 (1996)
8. I. Kawata, H. Kono, Y. Fujimura, J. Chem. Phys. **110**, 11152 (1999)
9. T. Otobe, M. Yamagiwa, J.-I. Iwata, K. Yabana, T. Nakatsukasa, Phys. Rev. B **77**, (2008)
10. K. Yabana, T. Sugiyama, Y. Shinohara, T. Otobe, G.F. Bertch, Phys. Rev. B **85**, (2012)
11. A. Becker, F.H.M. Faisal, J. Phys. B: At. Mol. Opt. Phys. **38**, R1–R51 (2005)
12. D.M. Volkov, Z. Phys. **94**, 250 (1935)
13. W.V. Houston, Phys. Rev. **57**, 184 (1940)
14. For a contemporary review, *Femtosecond Laser Filamentation*, S. L. Chin (Springer Series on Atomic, Optical, and Plasma Physics 55, 2010)
15. A. Dogariu, J.B. Michael, O. Scully, R.B. Miles, Science **331**, 442 (2011)
16. X. Zhang, R. Danylo, Z. Fan, P. Ding, C. Kou, Q. Liang, A. Houard, V. Tikhonchuk, A. Mysyrowicz, Y. Liu, Appl. Phys. B **53**, 126 (2020)
17. J. Yao, B. Zeng, H. Xu, G. li, W. Chu, J. Ni, H. Zhang, S. L. Chin, Y. Cheng, Z. Xu, Phys. Rev. A **84**, 051802(R) (2011)
18. Y. Zhang, E. Lötstedt, K. Yamanouchi, J. Phys. B **52**, (2017)
19. H. Xu, E. Lötstedt, A. Iwasaki, K. Yamanouchi, Nat. Commun. **6**, (2015)
20. J. Yao, S. Jiang, W. Chu, B. Zeng, C. Wu, R. Lu, Z. Li, H. Xie, G. Li, c. Yu, Z. Wang, H. Jiang, Q. Gong, Y. Cheng, Phys. Rev. Lett. **116**, 143007 (2016)
21. H. Li, M. Hou, H. Zang, Y. Fu, E. Lötstedt, T. Ando, A. Iwasaki, K. Yamanouchi, H. Xu, Phys. Rev. Lett. **122**, 013202 (2019)
22. Y. Kayanuma, S. Fukuchi, J. Phys. Soc. Jpn. **53**, 1869 (1984)

23. A. Yasui, T. Uozumi, Y. Kayanuma, Phys. Rev. B **72**, (2005)
24. Y. Kayanuma, K. Saito, Phys. Rev. A **77**, 010101 (R) (2008)
25. For a review of the Floquet engineering in periodically driven systems, see M. Holthaus, J. Phys. B: At. Mol. Opt. Phys. **49**, 013001 (2016). I thank T. N. Ikeda, for drawing my attention to this work.
26. T. Barbec, F. Krausz, Rev. Mod. Phys. **72**, 545 (2000)
27. A.D. Bandrauk, S. Barmaki, S. Chelkowski, G.L. Kamta, progress in ultrafast intense laser science III, Chap. 9, in *Springer Series in Chemical Physics*, eds. by K. Yamanouchi, S.L. Chin, P. Agostini, G. Ferrante
28. P.B. Corkum, Phys. Rev. Lett. **71**, 1995 (1993)
29. M. Lewenstein, Ph. Balcou, M. Yu. Ivanov, Anne L'Huillier, P.B. Corkum, Phys. Rev. A **49**, 2117 (1994)
30. G. Vampa, C.R. McDonald, G. Orlando, P.B. Corkum, T. Bravec, Phys. Rev. B **91** (2015)
31. D. Golde, T. Meier, S.W. Koch, Phys. Rev. B **77**, (2008)
32. T. Tamaya, A. Ishikawa, T. Ogawa, K. Tanaka, Phys. Rev. Lett. **116**, (2016)
33. H. Yamane, S. Tanaka, Symmetry Basel **10**, 313 (2018)
34. T.N. Ikeda, K. Chinzei, H. Tsunetsugu, Phys. Rev. A **98**, (2018)
35. See for example, M. I. Katsnelson, *Graphen* (Cambridge University Press, Cambridge, 2013)
36. Y. Mizumoto, Y. Kayanuma, A. Srivastava, J. Kono, A.H. Chin, Phys. Rev. B **74** (2006)
37. See for example, C. Yu, S. Jiang, R. Lu, Adv. Phys. **4**, 1562982 (2019)
38. O. Schubert, M. Hohenleutner, F. Langer, E. Urbanek, C. Lange, U. Huttner, D. Golde, T. Meier, M. Kira, S.W. Koch, R. Huber, Nat. Photonics **8**, 119 (2014)
39. K. Chinzei, T.N. Ikeda, Phys. Rev. Res. **2**, (2020)
40. G. Orland, T. Ho, S. Chu, J. Opt. Soc. Am. **37**, 1540 (2020)
41. I. Floss, C. Lemell, G. Wachter, V. Smejkal, S.A. Sato, X.-M. Tong, K. Yabana, J. Burgdörfer, Phys. Rev. A **97**, 011401(R) (2018)
42. S. Ghimire, D.A. Reis, Nat. Phys. **15**, 10 (2019)
43. D.H. Dunlap, V.M. Kenkre, Phys. Rev. B **34**, 3625 (1986)
44. M. Holthaus, Phys. Rev. Lett. **68**, 351 (1992)